Hindawi
Shock and Vibration
Volume 2020, Article ID 6651713, 11 pages
https://doi.org/10.1155/2020/6651713

Research Article

Acceleration Frequency Characteristics of the Freight-Train-Induced Vibration of the Beijing-Harbin Railway Subgrade

Yingying Zhao,[1,2,3] **Xianzhang Ling**,[4] **Ziyu Wang**,[5] **Weiming Gong**,[1,2] **and Guoyu Li**[3]

[1]*Key Laboratory of Concrete and Prestressed Concrete Structures of Ministry of Education, Southeast University, Nanjing 211189, Jiangsu, China*
[2]*School of Civil Engineering, Southeast University, Nanjing 211189, Jiangsu, China*
[3]*State Key Laboratory of Frozen Soil Engineering, Northwest Institute of Eco-Environment and Resources, Lanzhou 730000, Gansu, China*
[4]*School of Civil Engineering, Qingdao University of Technology, Qingdao 266033, Sandong, China*
[5]*School of Ecological Environment, Hainan Tropical Ocean University, Sanya 572022, Hainan, China*

Correspondence should be addressed to Ziyu Wang; zywang@hntou.edu.cn

Received 2 October 2020; Revised 13 October 2020; Accepted 10 November 2020; Published 23 November 2020

Academic Editor: Guangchao Zhang

The vibration acceleration during a freezing period was monitored in the Beijing-Harbin railway subgrade, and its frequency characteristics were studied. The results show the following. (1) The vibration acceleration frequency of the railway subgrade was divided into three main bands: the first frequency band is caused by the vehicle wheelbase, the second frequency band is caused by the sleeper spacing, and the third frequency band is mainly affected by the track irregularity spectrum and site structure. (2) The fitted dominant frequency, as can be seen from the monitored results, is in good agreement with the calculated value from the vibration frequency calculation formulas. (3) From the monitoring, it can be seen that train type, traveling speed, and train formation have a significant influence on the dominant frequencies of the first and second bands. Train formation, load, and distance from the track have a great influence on the amplitude of each frequency band.

1. Introduction

A railway subgrade suffers from periodic freezing-thawing cycles, as well as from the train vibration load, and these are the main reasons for roadbed debilitation in seasonally frozen regions. With the development of modern computers and the further application of finite-element numerical calculation methods, research of numerical calculation methods on the subgrade vibration has gradually deepened. Several scholars established a three-dimensional dynamic model to simulate the subgrade structure and track system, predicting the vibration response, and compared the results with those from field monitoring [1–4]. In model tests, one or more fixed points are applied with harmonic load to simulate the dynamic response and accumulated settlement of high-speed railway roadbeds under the action of train load. To apply moving loads, Momoya et al. [5] built a 1 : 5 indoor model test of ballasting track. Diyaljee [6] and Huang et al. [7] represented the magnitude of the train load and traveling speed through the amplitude and frequency of simple harmonic load. Al Shaer et al. [8] and Brown et al. [9] simulated the moving train load through multiple actuators. In field testing, the Swedish National Railway Authority tested the vibration of the X2000 high-speed train when it was running on soft ground and determined the critical speed in 1998 [10]. Other scholars have carried out field monitoring of several high-speed lines in China, such as the Qin-Shen [11–14], Beijing-Tianjin [15], Wu-Guang [16–18], and He-Ning [19] lines, with the tests covering wheel-rail interaction, dynamic response of the track system,

environmental vibration caused by the train load, and accumulated settlement of the subgrade. The results include the influence of train speed on the amplitude-frequency characteristics of roadbed vibration acceleration and the attenuation law of vibration acceleration amplitude and the distribution law of dynamic response and natural frequency. Xia [20] studied the vibration and environmental noise of surrounding buildings caused by traffic load. Ling et al. [21–23] conducted field monitoring of the vibration acceleration of a railway subgrade and analyzed the amplitude-frequency characteristics of acceleration in a frozen region.

In summary, the research results that have been published on acceleration monitoring of railway subgrades have mainly concentrated on permafrost regions and high-speed railways, and there are few studies on acceleration monitoring of railway subgrades in seasonally frozen regions. In addition, to the best of our knowledge, no report on the subgrade vibration spectrum caused by heavy trucks exists. In view of this, the acceleration spectrum characteristics caused by heavy freight trains in typical seasonally frozen regions are studied in this paper with the aim of providing the objective basis for railway subgrade design, prevention of debilitation, and disaster assessment in seasonally frozen regions.

2. Monitoring Methods

2.1. Information from Field Experiments. Harbin, located in Northeast China, is the provincial capital with the highest latitude and lowest temperature in China. The maximum temperature in summer exceeds 37°C, and the minimum temperature in winter is below −35°C. The maximum freezing depth is approximately 1.8–2 m. The monitoring section is located at k1229 + 095 of Beijing-Harbin railway. There are eight measuring points in the monitoring section located at the rail ($P1$), sleeper ($P2$), shoulder ($P3$), embankment ($P4$), embankment ($P5$), slope angle ($P6$), site ($P7$), and another site ($P8$). The geometry of the monitoring section, measurement-point layout, and stratigraphic structure are shown in Figure 1.

The monitoring instrument adopts an 891-2 vibration measuring instrument, which was developed by the Institute of Engineering Mechanics of the National Seismological Administration. The passband is 0.5–80 Hz, and the acceleration resolution is 1×10^{-5}. The acquisition equipment applies the INV306 signal acquisition and analysis system developed by China Oriental Vibration and Noise Technology Research Institute.

2.2. Introduction of the Monitoring Train. The vibration acceleration of nine freight trains was monitored. Vehicle parameter information such as vehicle number, vehicle structure, vehicle grouping, driving speed, half of bogie spacing, half of inflexible bogie wheelbase, and sleeper space is shown in Table 1. The schematic of the interaction force between the vehicle and the sleeper is presented in Figure 2.

3. Results and Discussion

The time-frequency characteristics of acceleration in a freezing period were analyzed with a typical freight train as an example. Since point $P1$ is placed on the track, point $P2$ is placed on the sleeper and point $P3$ (the shoulder) on the loose gravel. Thus, the monitoring results of nine typical freight trains at points $P4$–$P8$ were mainly analyzed in this paper. The research results include acceleration-time history, spectrum characteristics, and influencing factors of the freight trains.

3.1. Time Histories of the Acceleration Response. Figure 3 shows partial monitoring results, including the acceleration-time-history curves of trains 11114, 11138, and 40194 at point $P4$ and train 11022 at points $P4$–$P7$. It can be seen from the graph that the time-history curve of the vehicle is influenced by vehicle formation, load, and speed. The peak and valley of the acceleration-time-history curve of each vehicle appear in pairs. At the point nearest to the center of the rail ($P4$), the peak time of the acceleration-time-history curve is in clear correspondence to the train wheel. Far from the center of the line ($P7$), the peak acceleration is small and spindle-shaped. It can be seen that the structural vibration caused by a train passing is transmitted from the track to the subgrade, and the vibration intensity is obviously weakened after passing through sleepers and ballast beds, but its interaction with the wheel and rail still appears correspondingly.

3.2. Acceleration Spectrum Analysis. The internal vibration frequency of railway subgrades is affected by many factors, such as subgrade structure, vehicle type, driving speed, and track irregularity spectrum. Formulas (1)–(3) are used to calculate the vibration frequency caused by the vehicle fixed distance, bogie fixed wheelbase, and sleeper spacing:

$$f_{ci,s} = \frac{i \times v}{2 \times l_c} \ (i = 1, 2, 3, \ldots), \tag{1}$$

$$f_{ti,s} = \frac{i \times v}{2 \times l_t} \ (i = 1, 2, 3, \ldots), \tag{2}$$

$$f_{si,s} = \frac{i \times v}{2 \times l_s} \ (i = 1, 2, 3, \ldots), \tag{3}$$

where v represents the train speed, l_c half of vehicle fixed distance, l_t half of bogie fixed wheelbase, and l_s the sleeper space.

The frequency spectrum is obtained by the fast Fourier transform of acceleration-time-history data. Because the acceleration spectrum is discrete, the frequency bands were fitted separately, and the peak fitting method uses the Gaussian function to fit the monitoring data. The abscissa of the center point of the Gaussian function represents the dominant frequency, and the function width represents the bandwidth. In this paper, nine groups of spectrograms for

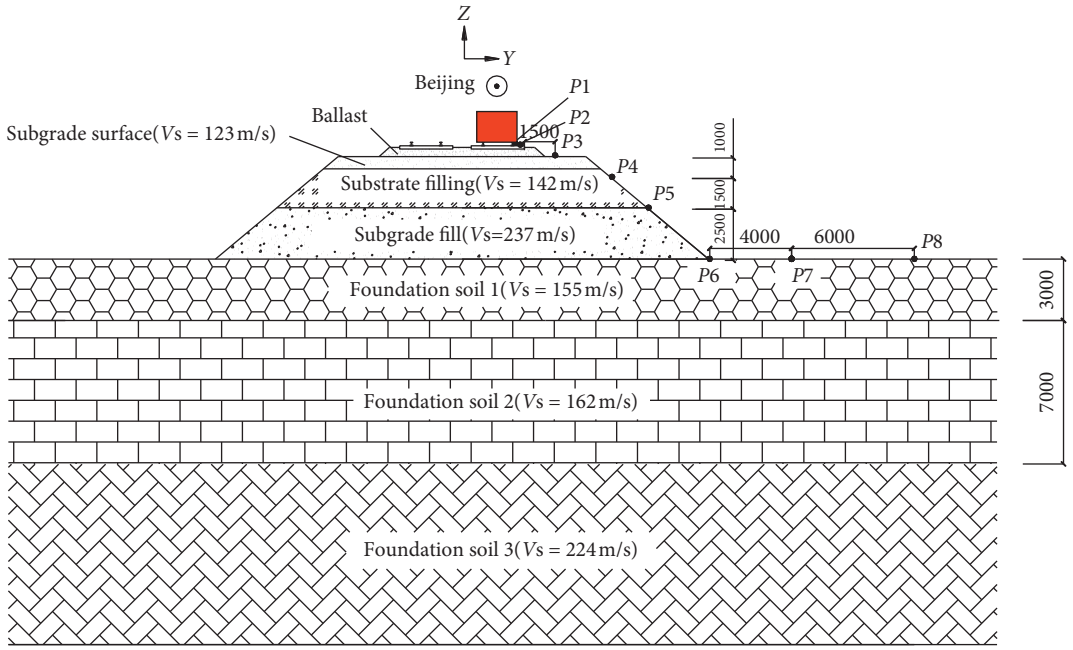

Figure 1: Layout of measuring points for the cross section of the monitoring section.

Table 1: Parameters of the monitoring train.

Train	Train structure	Train frame	Traveling speed (km/h)	l_c (m)	l_t (m)	l_s (m)
11018		2 + 64	65			
11404		2 + 56	61			
11114		2 + 68	70			
11138		2 + 66	70			
40194	Primary suspension	1 + 31	60	4.25	0.915	0.556
111040		2 + 66	60			
11020		2 + 62	67			
40196		1 + 41	56			
11022		2 + 60	65			

$2l_c$, vehicle fixed distance; $2l_t$, bogie fixed wheelbase; l_s, sleeper space.

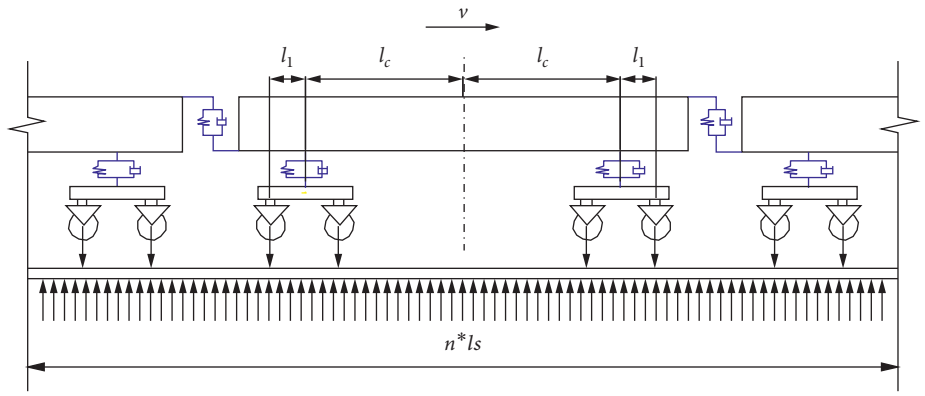

Figure 2: Schematic of the interaction force between the vehicle and the sleeper ($2l_c$, vehicle fixed distance; $2l_t$, bogie fixed wheelbase; l_s, sleeper space; n, number of sleepers).

monitoring freight vehicles are given, as shown in Figure 4. Taking freight train 11018 (train formation 2 + 64; traveling speed $v = 65$ km/h) as an example, it can be seen from Figure 4(a) that the acceleration spectrum curve includes three distinct frequency bands. The first frequency band is between 0 and 20 Hz, and the dominant frequency of the

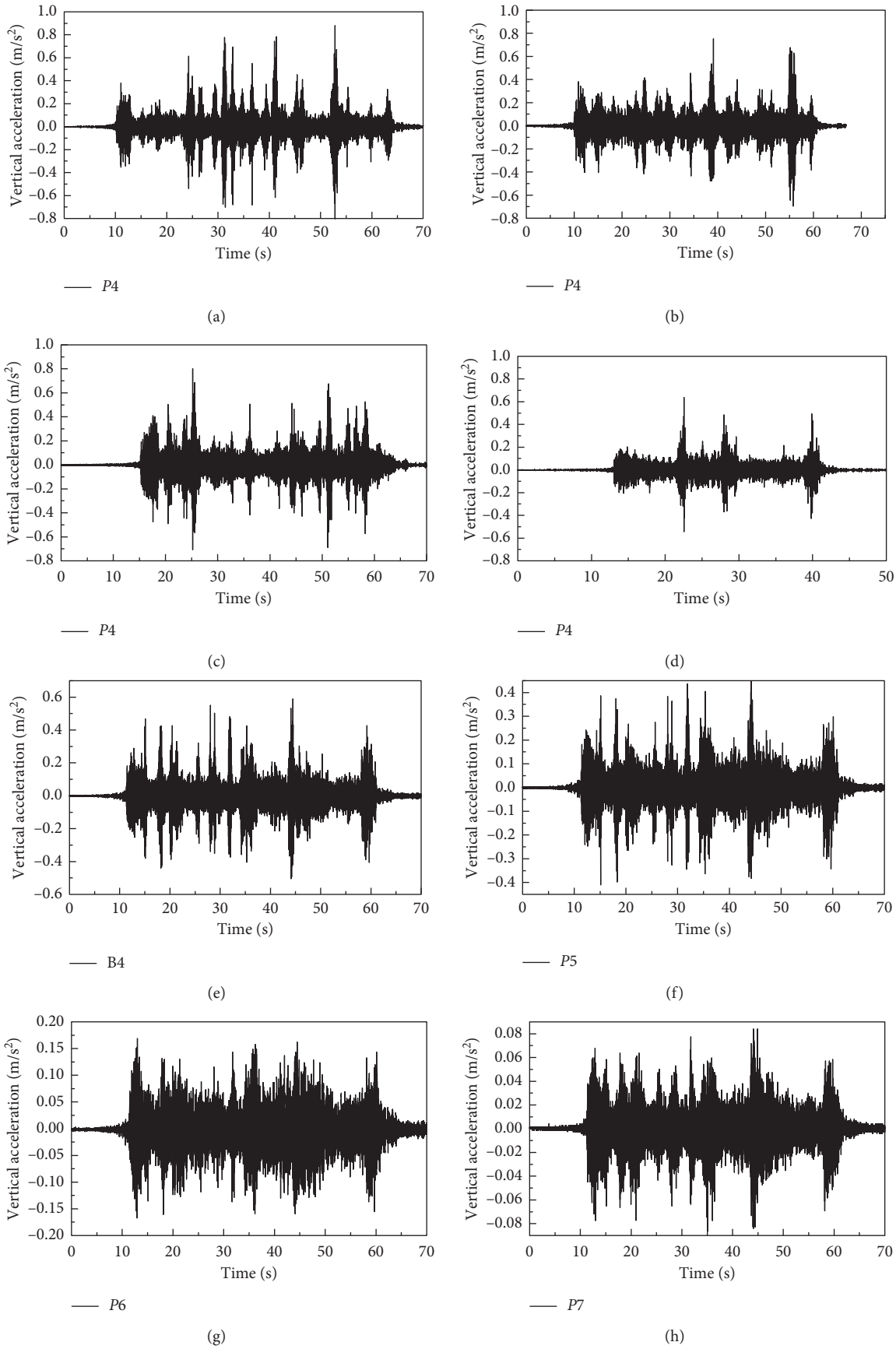

Figure 3: Acceleration-time-history curves. (a) Freight train 11404. (b) Freight train 11114. (c) Freight train 11138. (d) Freight train 40194. (e) Freight train 11022. (f) Freight train 11022. (g) Freight train 11022. (h) Freight train 11022.

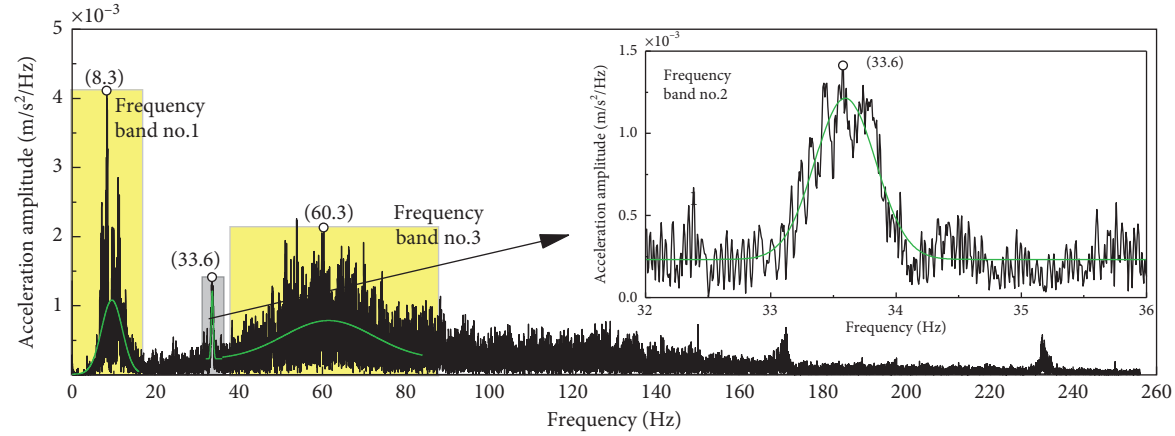

(a)

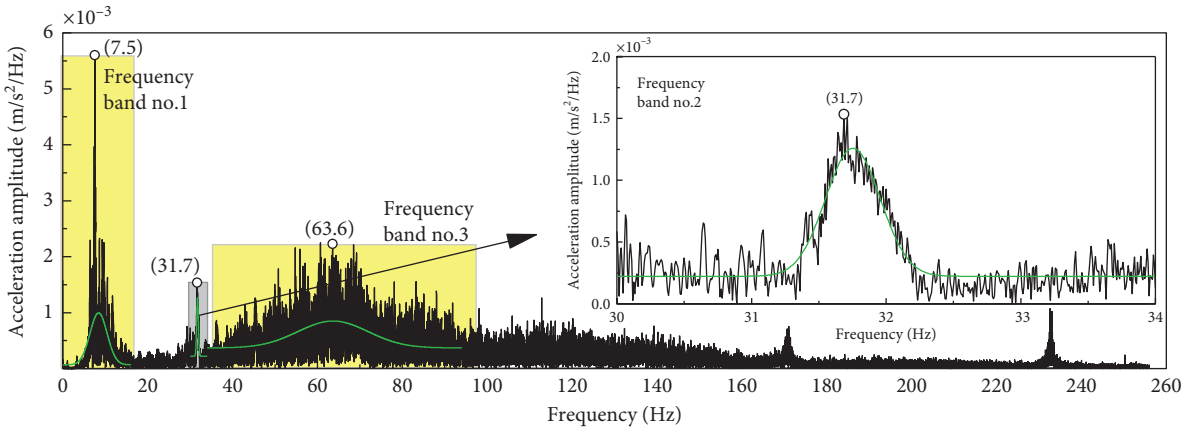

(b)

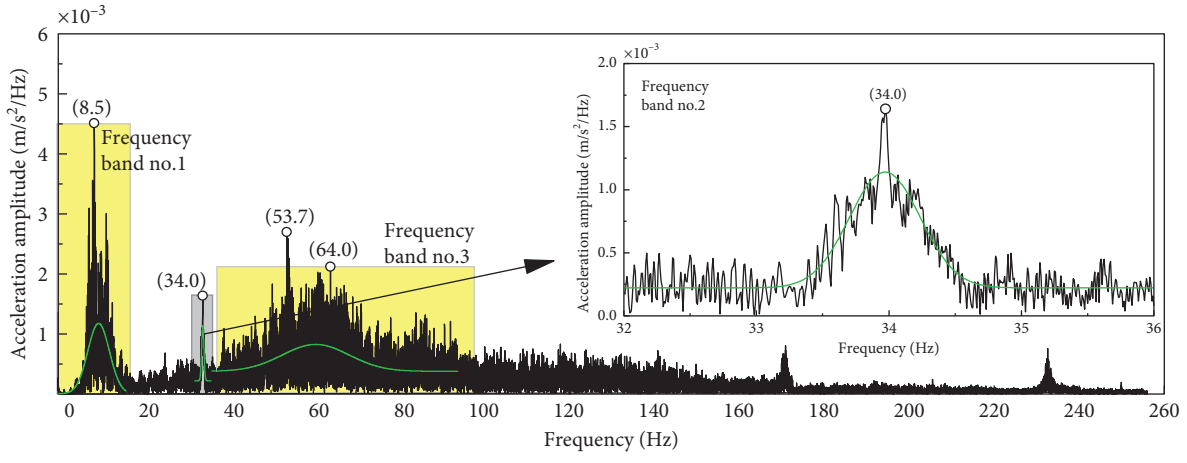

(c)

Figure 4: Continued.

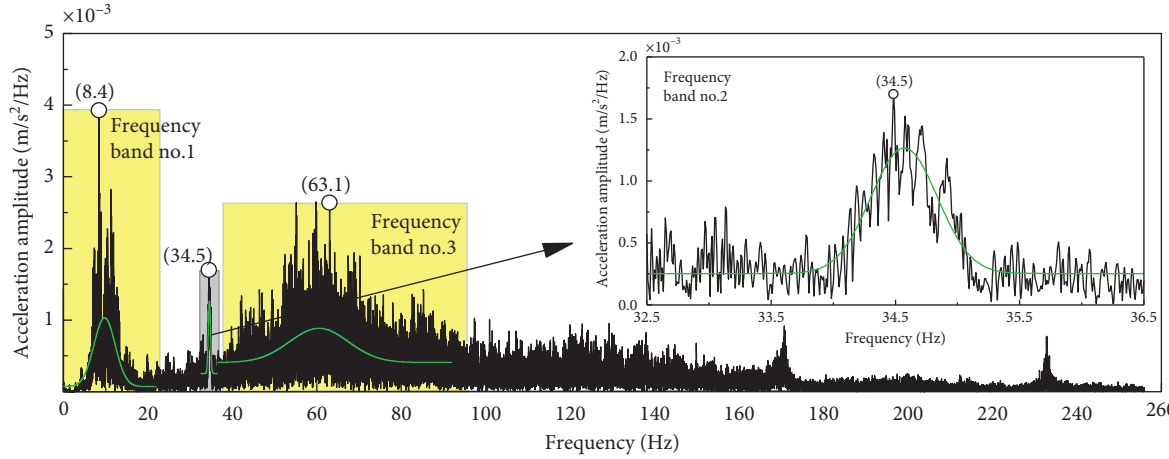

(d)

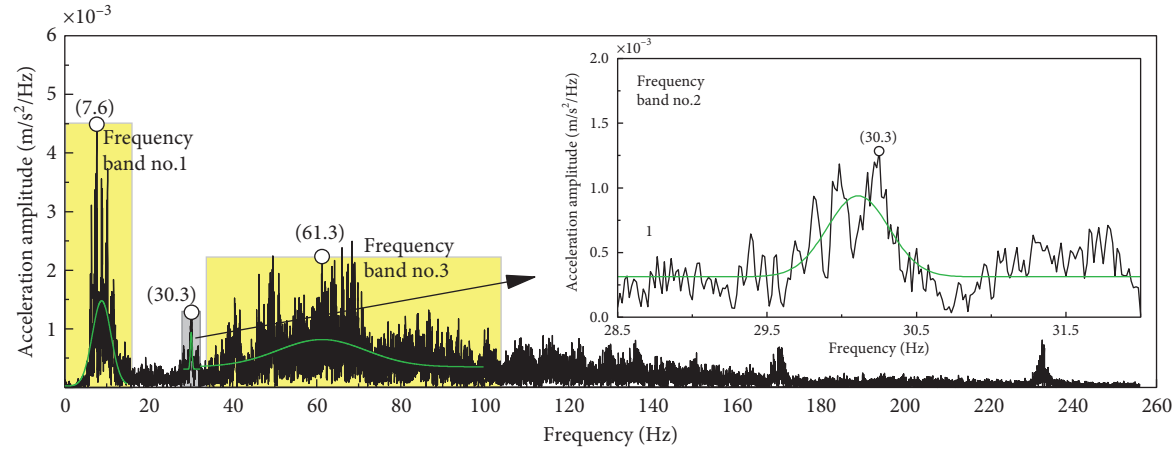

(e)

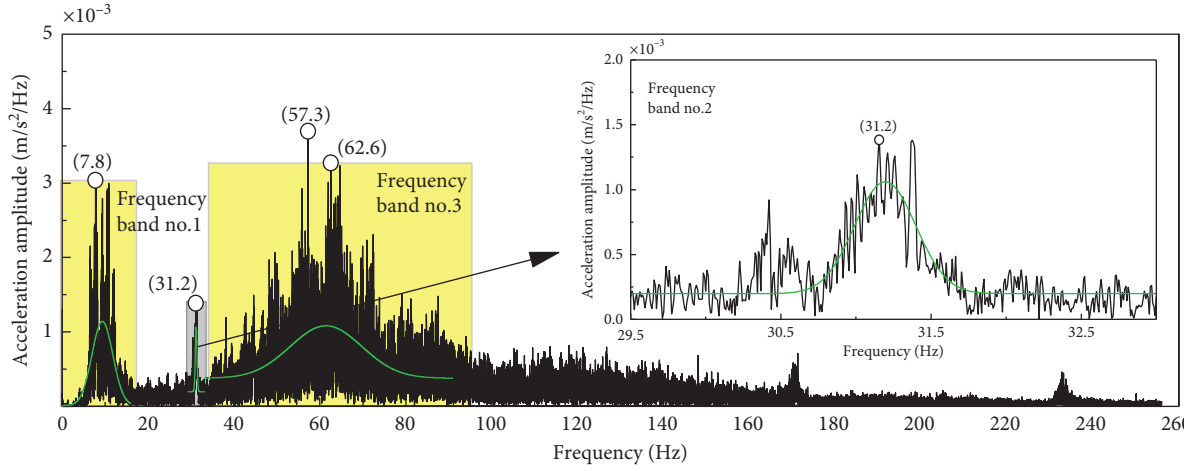

(f)

Figure 4: Continued.

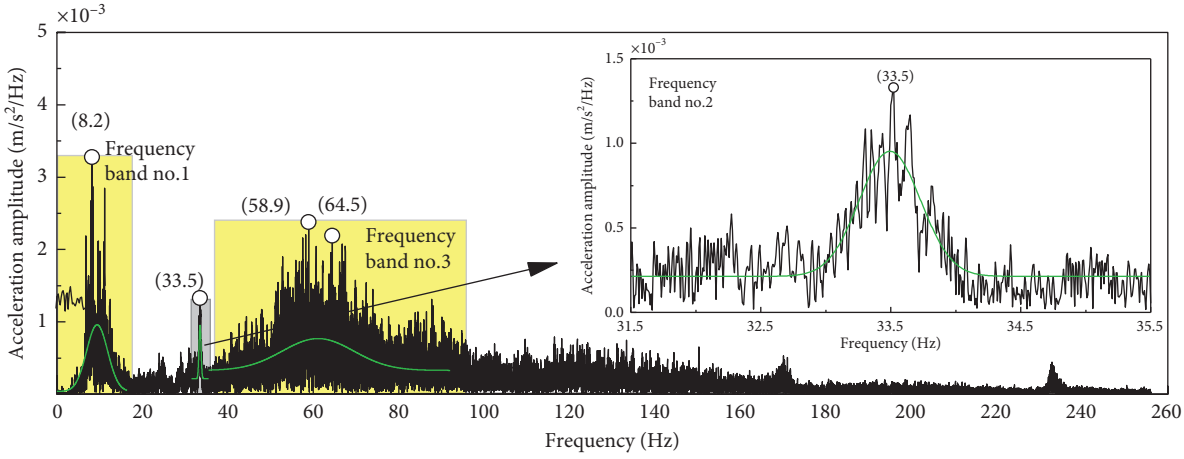

(g)

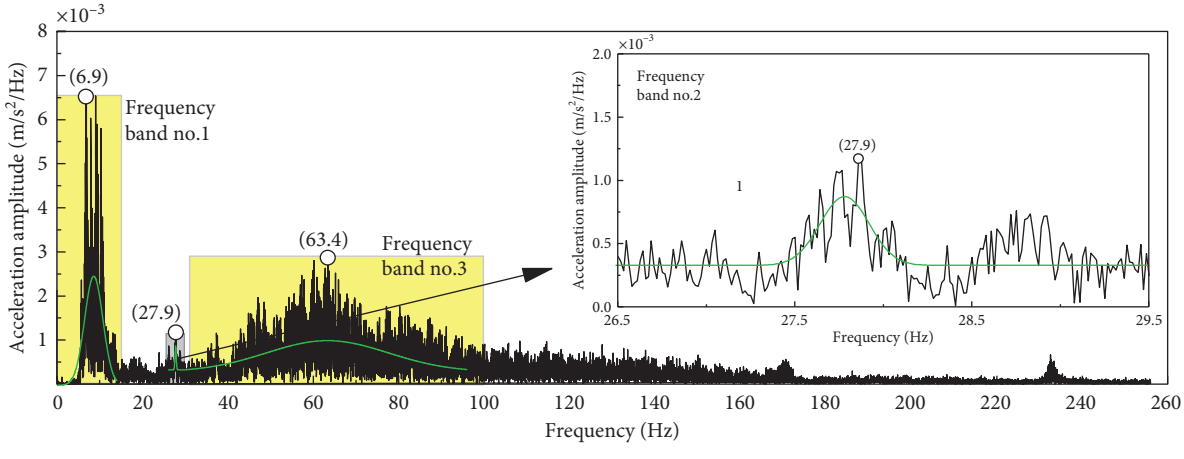

(h)

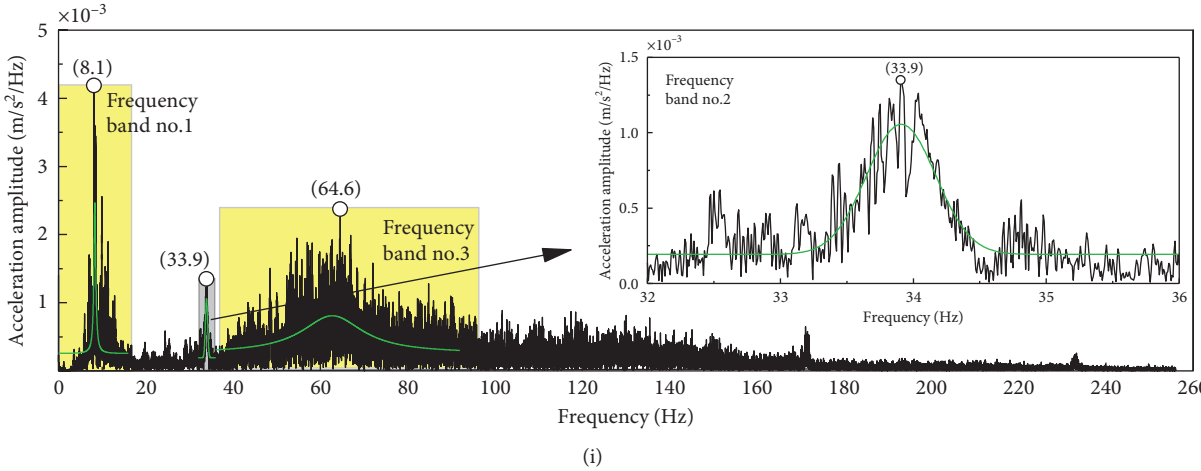

(i)

Figure 4: Frequency spectra of acceleration at *P*4. (a) Freight train 11018. (b) Freight train 11404. (c) Freight train 11114. (d) Freight train 11138. (e) Freight train 40194. (f) Freight train 111040. (g) Freight train 11020. (h) Freight train 40196. (i) Freight train 11022.

band is $f1$, $c = 8.3$ Hz; the second frequency band is between 25 and 35 Hz, and the corresponding dominant frequency is $f2$, $c = 33.6$ Hz; and the third obvious frequency band is wider, between 35 and 150 Hz, and has the largest vibration energy. The dominant frequency of the band is $f3$, $c = 60.3$ Hz. As can be seen from the graph, each frequency band tends to exhibit normal symmetrical distribution; that is, within each frequency band, the peak frequency is located near the center of the frequency band.

The main frequency caused by the vehicle fixed distance, bogie fixed wheelbase, and sleeper space was calculated by formulas (1)–(3) as $f_{c1,s} = 1 \times (65/3.6)/(2 \times 4.25) = 2.1$ Hz.

This dominant frequency is not obvious in the spectrum (Figure 4). If the spectrum is amplified locally, it can be found that there is a narrow frequency band near 2 Hz, and the corresponding amplitude is small, which is the reason an in-depth study of the main frequency was not made. $f_{t1,s} = 1 \times (65/3.6)/(2 \times 0.915) = 9.9$ Hz, which is similar to the dominant frequency of the first band of 8.3 Hz. $f_{s1,s} = 1 \times (65/3.6)/0.556 = 32.5$ Hz, which is similar to the second-band dominant frequency of 33.6 Hz.

Figures 4(a)–4(i) show that the freight train has a larger load and more carriages, and the speed of each vehicle is between 60 and 70 km/h. The acceleration frequencies of each train are mainly divided into three bands: the first band's bandwidth is between 0 and 20 Hz, and the dominant frequency is between 8 and 10 Hz; it is mainly caused by the vehicle fixed distance. The second band's bandwidth is between 25 and 35 Hz, and the dominant frequency is near 30 Hz; it is mainly caused by the sleeper space. The bandwidth of the third band is the largest, ranging from 35 to 150 Hz, the dominant frequency is between 50 and 60 Hz, and the vibration energy is the largest. This frequency band is mainly determined by the track irregularity spectrum and field conditions.

Considering that the data of the acceleration spectrogram are discrete and each frequency band basically exhibits normal distribution, the peak values of each frequency band are fitted separately. The frequencies of nine freight trains at different measuring points $P4$–$P8$ and different frequency bands were peak-fitted separately, and the corresponding peak frequency was taken as the fitted dominant frequency of the band, drawing the relationship between the fitted dominant frequency (FDF) of each band and the vehicle speed, as shown in Figure 5. It can be seen from the graph that, in the three frequency bands, the linear relationship between the FDF and the vehicle speed has been monotonously increased. Compared with the growth rate of each FDF, it is found that the FDF in the second frequency band clearly increases with increasing driving speed, and the slope is 0.41. The first and third fitting dominant frequencies are not obvious with increasing speed, and the slope is 0.06.

3.3. Influence of the Train Formation. A one-third-octave spectrum is an important means of signal analysis that has the characteristics of wide bandwidth and few spectral lines. To facilitate comparison, the frequency characteristics of acceleration were analyzed by a one-third-octave spectrum.

As can be seen from Figure 6, the dominant frequencies of each vehicle in the first and second bands are different due to the influence of driving speed, while the dominant frequencies in the third band are basically the same. The acceleration amplitudes corresponding to dominant frequencies in each frequency band are clearly different. This is caused by the different number of carriages. Train 11040's acceleration amplitude is the maximum, with a vehicle formation of 2 + 66 and amplitude of approximately 5.8 ms^{-2}/Hz; train 40194's acceleration amplitude is the smallest, and its vehicle formation is 1 + 31 followed by vehicle 40196, the vehicle formation of which is 1 + 41. It can be seen that vehicle formation has a significant impact on vibration amplitude.

3.4. Influence of the Train Type. Figure 7 shows the one-third-octave spectrum for monitoring the vertical acceleration of passenger and freight trains at $P4$. Owing to the different sizes of vehicle structures, the frequency spectra of freight and passenger trains are quite different. In the first frequency band, the dominant frequencies of freight and passenger trains are approximately 8 and 10 Hz, respectively; in the second frequency band, the dominant frequencies of freight trains are approximately 30 Hz, while those of passenger trains are not obvious in this frequency band; and in the third band, the dominant frequencies are all approximately 60 Hz.

This is because the structure size of freight and passenger trains is different, the number of carriage groups is much larger than that of passenger trains, and the driving speed is less than that of passenger trains. Therefore, the dominant frequency in the first and second bands of passenger trains is slightly larger than that of freight trains, but the acceleration amplitude is smaller.

3.5. Influence of the Direction. To analyze the influence of the vibration direction on dominant frequencies in each frequency band, the vibration frequencies of nine trains in the X-, Y-, and Z-directions are compared, as shown in Figure 8. It can be seen from the figure that the dominant frequencies of the X- and Y- directions are basically the same, with obvious differences from the Z-direction. In the first band, the dominant frequencies in the Z-direction are slightly smaller than those in the X- and Y-directions; in the second band, the dominant frequencies in all three directions are basically the same, approximately 30–35 Hz; and in the third band, the dominant frequencies in the Z-direction are near 60 Hz, while the dominant frequencies in the X- and Y-directions are near 100 Hz. The amplitude of acceleration in the Z-direction is obviously larger than that in the X- and Y-directions. This difference is caused by different subgrade structures in different directions.

3.6. Influence of the Distance to the Rail. Figure 9 shows the one-third-octave spectrum of freight train 11022 at measuring points $P4$–$P8$. It can be seen that the dominant frequencies of each measuring point are basically the same in three bands, i.e., approximately 8–10, 30–35, and 60 Hz. The acceleration amplitude of each measuring point in the three frequency bands decreases with increasing distance from the center of the rail due to the filtering of the site. In the first band, the acceleration amplitude at point $P4$ is approximately 2.6 ms^{-2}/Hz, and at point $P8$, the acceleration amplitude decreases to 1.1 ms^{-2}/Hz. In the second band, the acceleration amplitude at point $P4$ is approximately 1.3 ms^{-2}/Hz, and at point $P8$, it decreases to 0.4 ms^{-2}/Hz. In the third band, the acceleration amplitude at point $P4$ is approximately 4.2 ms^{-2}/Hz, and the amplitude decreases to 0.4 ms^{-2}/Hz at point $P8$. It can be seen that the dominant

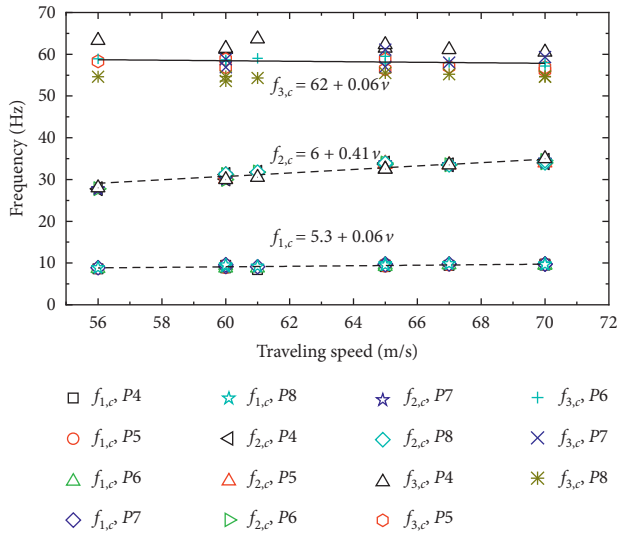

Figure 5: Relationship between traveling speed and fitted dominant frequency.

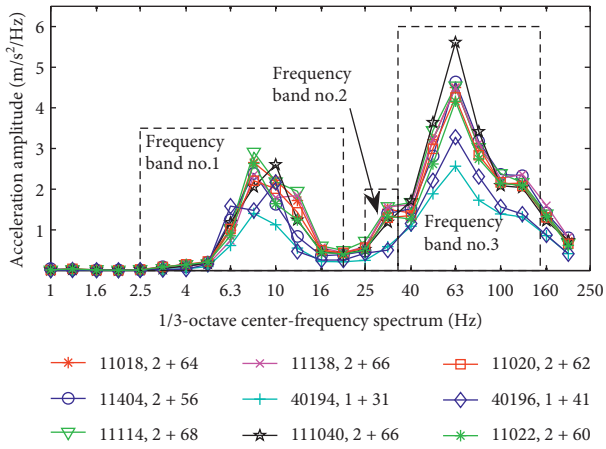

Figure 6: One-third-octave center-frequency spectrum induced by different vehicle marshallings (*P*4).

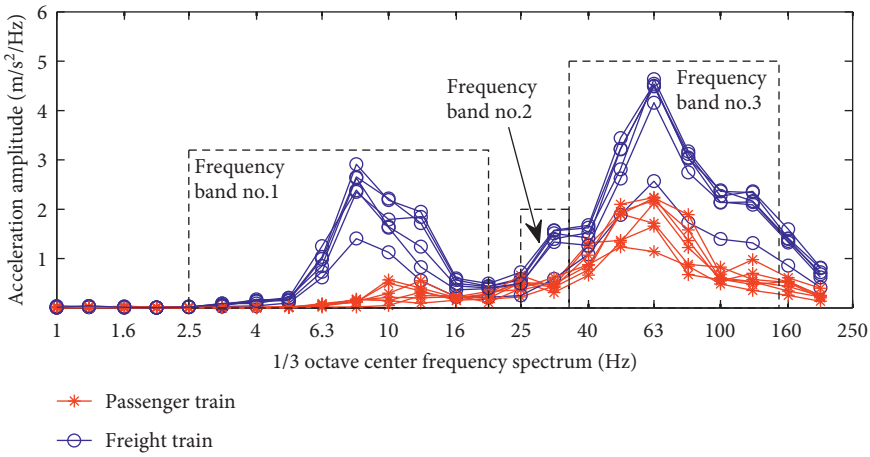

Figure 7: One-third-octave center-frequency spectrum induced by different types of trains (*P*4).

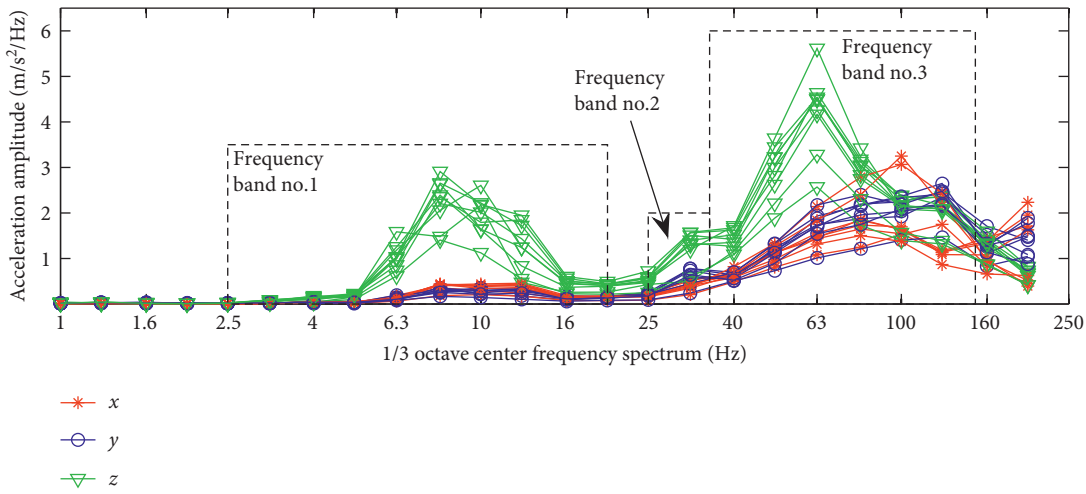

Figure 8: One-third-octave center-frequency spectrum induced by different directions (*P*4).

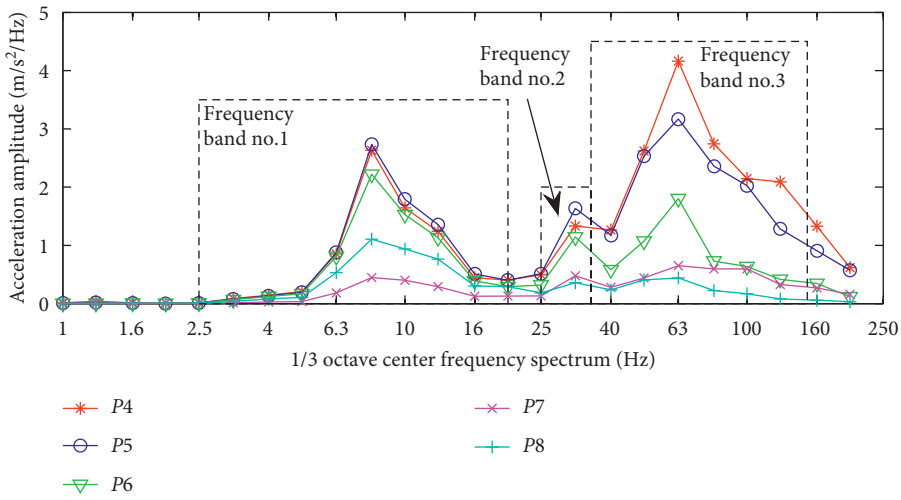

Figure 9: One-third-octave center-frequency spectrum induced by different distances (train 11022).

frequency of the acceleration vibration is almost unchanged, the amplitude attenuation is obvious, and the attenuation rate of the third band is the largest with increasing distance from the orbit.

4. Conclusions

Through monitoring the acceleration of freight trains running on China's Harbin railway, amplitude-frequency characteristics of vibration acceleration and its influencing factors are described, and the following conclusions are drawn:

(1) The acceleration frequencies of railway subgrades caused by freight trains are divided into three main frequency bands. The first frequency band is between 0 and 20 Hz, and the dominant frequency near $f_{t1,s} = 1 \times v/(2 \times l_t)$; the second frequency band distribution is between 25 and 35 Hz, and the dominant frequency near $f_{s1,s} = 1 \times v/l_s$; and the third frequency band is between 35 and 150 Hz, and the vibration energy is the largest.

(2) Because the acceleration spectrum is discrete, the three frequency bands were fitted with peak values separately, and it can be seen that the FDF in the second frequency band clearly increases with increasing driving speed, and the slope is 0.41; the first and third FDFs increase slightly with increasing speed.

(3) Owing to the different sizes of the vehicle structure, the frequency spectra of freight and passenger trains are quite different: in the first frequency band, the dominant frequencies are slightly different, and in the second and third bands, the dominant frequencies are all approximately 30 and 60 Hz.

(4) Vibration amplitude-frequency characteristics of freight trains are affected by train type, traveling speed, train formation, vibration direction, distance from the track, track irregularity spectrum, site

structure, and other factors. Among these, train type, traveling speed, and train formation have a significant influence on the dominant frequencies of the first and second bands. Train formation and distance from the track have obvious effects on the amplitude of each frequency band.

Data Availability

Some data used during the study are available from the corresponding author upon request.

Conflicts of Interest

The authors declare no conflicts of interest.

Acknowledgments

This research was supported by the State Key Laboratory of Frozen Soil Engineering (Grant no. SKLFSE201907), Key Research and Development Projects in Hainan Province (Grant no. ZDYF2017100), National Key R&D Program of China (Grant no. 2018YFC1505300), and National Major Scientific Instruments Development Project of China (Grant no. 41627801).

References

[1] P. Galvín, A. Romero, and J. Domínguez, "Vibrations induced by HST passage on ballast and non-ballast tracks," *Soil Dynamics and Earthquake Engineering*, vol. 30, no. 9, pp. 862–873, 2010.

[2] A. Khoubani and M. M. Ahmadi, "Discussion on the paper entitled: numerical modeling of traffic-induced ground vibration," *Computers and Geotechnics*, vol. 47, p. 102, 2013.

[3] F. C. Xue and J. M. Zhang, "Attenuations of acceleration spectra of high-speed railway embankment subjected to moving loads," *Rock and Soil Mechanics*, vol. 36, no. 1, pp. 445–451, 2015.

[4] G. Kouroussis, O. Verlinden, and C. Conti, "Free field vibrations caused by high-speed lines: measurement and time domain simulation," *Soil Dynamics and Earthquake Engineering*, vol. 31, no. 4, pp. 692–707, 2011.

[5] Y. Momoya, E. Sekine, and F. Tatsuoka, "Deformation characteristics of railway roadbed and subgrade under moving-wheel load," *Soils and Foundations*, vol. 45, no. 4, pp. 99–118, 2005.

[6] V. Diyaljee, "Discussion of "Stress-Strain degradation response of railway ballast stabilized with geosynthetics" by buddhima indraratna and sanjay nimbalkar," *Journal of Geotechnical and Geoenvironmental Engineering*, vol. 139, no. 12, pp. 2232-2233, 2013.

[7] S. Liu, H. Huang, T. Qiu, and J. Kwon, "Effect of geogrid on railroad ballast particle movement," *Transportation Geotechnics*, vol. 9, pp. 110–122, 2016.

[8] A. Al Shaer, D. Duhamel, K. Sab, G. Foret, and L. Schmitt, "Experimental settlement and dynamic behavior of a portion of ballasted railway track under high speed trains," *Journal of Sound and Vibration*, vol. 316, no. 1-5, pp. 211–233, 2008.

[9] S. F. Brown, B. V. Brodrick, N. H. Thom, and G. R. McDowell, "The nottingham railway test facility, UK," *Proceedings of the Institution of Civil Engineers - Transport*, vol. 160, no. 2, pp. 59–65, 2007.

[10] C. Madshus and A. M. Kaynia, "High-speed railway lines on soft ground: dynamic behaviour at critical train speed," *Journal of Sound and Vibration*, vol. 231, no. 3, pp. 689–701, 2000.

[11] Z. Y. Xue, L. Li, B. S. Liu et al., "Testing and analysis on vibration of subgrade for qinhuangdao-shenyang railway," *Chinese Journal of Rock Mechanics and Engineering*, vol. 24, no. 6, pp. 1067–1071, 2005.

[12] Z. Y. Nie, B. Ruan, and L. Li, "Testing and analysis on dynamic performance of subgrade of qinshen railway," *Journal of Vibration and Shock*, vol. 24, no. 2, pp. 30–32, 2005.

[13] G. Y. Gao, Z. Y. Li, S. J. Feng et al., "Experimental results and numerical predictions of ground vibration induced by high-speed train running on qinghuangdao- shengyang railway," *Rock and Soil Mechanics*, vol. 28, no. 09, pp. 1817–1822, 2007.

[14] W. M. Zhai, *Vehicle-track Coupling Dynamics*, Science Press, Beijing, China, 2007.

[15] S. G. Zhang, X. Kang, and X. B. Liu, "Characteristic analysis of the power spectral density of track irregularity on beijing-tianjin inter-city railway," *China Railway Science*, vol. 29, no. 05, pp. 25–30, 2008.

[16] S. B. Fan, *"Analysis on Experiment of Dynamic Response in Ballastless Track Subgrade of High Speed Railway*, Southwest Jiaotong University, Chengdu, China, 2010.

[17] C. Z. Qu, Y. H. Wang, L. M. Wei et al., "In-situ test and analysis of vibration of subgrade for wuhan-guangzhou high-speed railway," *Rock and Soil Mechanics*, vol. 33, no. 5, pp. 1451–1456, 2012.

[18] B. Chen, G. X. Chen, D. H. Zhu et al., "Experimental study of ground vibration caused by rail transit," *Journal of Disaster Prevention and Mitigation Engineering*, vol. 27, no. 3, pp. 312–317, 2007.

[19] D. W. Zheng, B. L. Wang, S. H. Zhou et al., "Study on vibration character of expansive Soil embankments with different rigidities along hefei-nanjing rapid railway," *Chinese Journal of Rock Mechanics and Engineering*, vol. 25, no. 2, pp. 4204–4208, 2006.

[20] H. Xia, *Traffic Induced Environmental Vibrations and Controls*, Science Press, Beijing, China, 2010.

[21] X. Ling, F. Zhang, Z. Zhu, L. Ding, and Q. Hu, "Field experiment of subgrade vibration induced by passing train in a seasonally frozen region of daqing," *Earthquake Engineering and Engineering Vibration*, vol. 8, no. 1, pp. 149–157, 2009.

[22] Z.-Y. Zhu, X.-Z. Ling, Z.-Y. Wang et al., "Experimental investigation of the dynamic behavior of frozen clay from the beiluhe subgrade along the QTR," *Cold Regions Science and Technology*, vol. 69, no. 1, pp. 91–97, 2011.

[23] Z. Y. Wang, X. Z. Ling, Z. Zhu, and F. Zhang, "Dominant frequencies of train-induced vibrations in a seasonally frozen region," *Cold Regions Science and Technology*, vol. 116, pp. 32–39, 2015.